Site-Selective Binding of Nanoparticles to Double-Stranded DNA *via* Peptide Nucleic Acid "Invasion"

Andrea L. Stadler,[†,⊥] Dazhi Sun,[‡,⊥] Mathew M. Maye,[§] Daniel van der Lelie,[†] and Oleg Gang[‡,*]

[†]Biology Department, and [‡]Center for Functional Nanomaterials, Brookhaven National Laboratory, Upton, New York 11973, United States, and [§]Department of Chemistry, Syracuse University, Syracuse, New York 13244, United States. [⊥]These authors contributed equally to this work.

ABSTRACT We demonstrate a novel method for by-design placement of nano-objects along double-stranded (ds) DNA. A molecular intercalator, designed as a peptide nucleic acid (PNA)−DNA chimera, is able to invade dsDNA at the PNA-side due to the hybridization specificity between PNA and one of the duplex strands. At the same time, the single-stranded (ss) DNA tail of the chimera, allows for anchoring of nano-objects that have been functionalized with complementary ssDNA. The developed method is applied for interparticle attachment and for the fabrication of particle clusters using a dsDNA template. This method significantly broadens the molecular toolbox for constructing nanoscale systems by including the most conventional not yet utilized DNA motif, double helix DNA.

KEYWORDS: gold nanoparticles · peptide nucleic acid · double-stranded DNA · nanoparticle assembly

The ability to organize nano-objects into well-defined architectures allows for the functional exploitation and harnessing of the unique properties of nanomaterials. In recent years, DNA has been successfully used as a programmable glue,[1,2] scaffold,[3,4] and selective and tunable mediator[5−8] for the precise organization of a variety of nanomaterials, including gold and silver nanoparticles,[9] quantum dots[10] and nanotubes[11] in clusters,[9,12] 2D arrays,[3,4,13,14] and 3D superlattices.[5−8] Despite this variety of assembly approaches, the majority of the current strategies for programmable DNA-based assembly on a nano- and microscale[15−17] rely on single-stranded DNA (ssDNA) directed hybridization. In brief, particles, for example gold nanoparticles (AuNPs), are typically functionalized with ssDNA, and specific Watson−Crick base-pairing is used to direct the binding of DNA-functionalized AuNPs to complementary ssDNA from another particle or to DNA scaffold arrays. Respectively, this allows for the formation of discrete clusters, 3D aggregates, or particle positioning on 2D periodic arrays. The underlying strategy of these nanoparticle organizations relies on the use of single-stranded DNA, either to connect particles or to be used as an elemental block for building DNA scaffolds. This reflects the principal limitation of these approaches, which require ssDNA as an initial material for system fabrication.

On the other hand, the most common and tailorable DNA material, double-stranded DNA (dsDNA) has not been used in nanotechnology to its full potential. Genetically modifiable dsDNA, which can be micrometers in length, can potentially serve as a highly addressable, tunable arbitrary template for particle positioning. However, one of the unresolved problems toward the application of dsDNA as a template for assembly is the absence of reliable methods for by-design site-selective placement of nano-objects on a given duplex. The sequence-selective pyrrole−imidazole polyamides have been used to target dsDNA on a 2D DNA tile array and allow for the precise positioning of streptavidin along the array. Polyamides sequence specifically bind the minor groove of dsDNA; however, they are limited in their sequence specificity and the length of the DNA sequence they target.[18]

Here we present a strategy for site-selective attachment of nanoparticles to dsDNA that might allow for the arbitrary organization of nano-objects. While recognition of ssDNA is readily achieved based on the principles of nucleic acid base-pairing, recognition of dsDNA is more challenging. Our approach uses a peptide nucleic acid (PNA)−DNA chimera to addressably target dsDNA. PNA is a synthetic mimic of DNA and RNA with a neutrally charged backbone, and has been shown to invade duplex DNA sequence specifically.[19−21] A PNA−DNA duplex is more stable than an analogous DNA−DNA duplex due to the reduced electrostatic repulsion provided by the neutral PNA backbone. Recently, several groups have demonstrated the use of PNA for fabrication of AuNP clusters,[22−27] including direct functionalization of AuNPs with PNA and

* Address correspondence to ogang@bnl.gov.

Received for review June 16, 2010 and accepted February 16, 2011.

Published online March 09, 2011
10.1021/nn101355n

PNA–DNA chimeras, nonspecific absorption of PNA to citrate-stabilized AuNPs, and the use of PNA as a linker for DNA-functionalized AuNPs. However, each of these methods relies on the single-stranded recognition of a DNA strand by a PNA strand.

In our approach, the PNA region of a PNA–DNA chimera (PNA–DNA-1) acts as a molecular intercalator

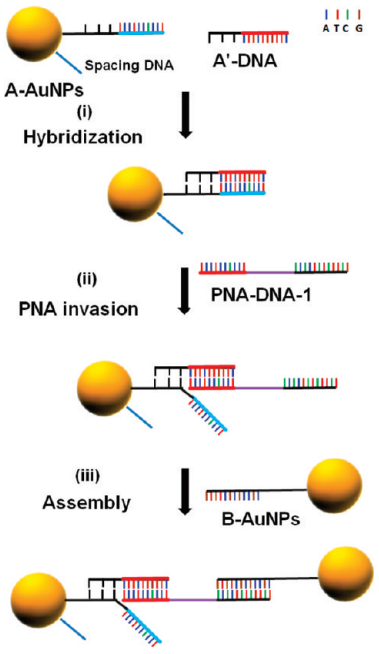

Figure 1. Schematic of noncomplementary particle–particle assembly. (i) A′-DNA hybridizes to the surface of A-DNA functionalized 10 nm AuNPs. Unhybridized A′-DNA is removed by centrifugation. (ii) PNA–DNA-1 is added and invades the duplex on the particle surface. (iii) Finally, B-AuNP is mixed with the A-AuNPs bearing bound PNA–DNA-1 on their surface, and nanoparticle aggregates are formed through the base-pair hybridization of B-AuNP with the 15 base DNA section of PNA–DNA-1.

to "invade" dsDNA at sequence-specific locations. PNA has long been used as a duplex invader in biological applications, such as transcription regulation and fluorescence imaging for *in situ* hybridization assays.[28,29] In nano-assembly, duplex invasion by a PNA–DNA chimera permits the subsequent attachment of nanoobjects or macromolecules at this location due to its recognition to the DNA side of the chimera. The utilization of PNA invasion offers a powerful way to organize nanoparticles using dsDNA templates and provides novel means for building nanoscale architectures. As a proof of concept, we investigated two scenarios that are applicable to a broad range of DNA-based nanofabrication approaches: (i) particle–particle assembly mediated by a PNA–DNA chimera, and (ii) positioning of particles on a dsDNA template using a PNA–DNA chimera.

RESULTS AND DISCUSSION

Our strategy for PNA-directed particle–particle assembly, depicted in Figure 1, uses a 10 base PNA and 15 base DNA (PNA–DNA-1) chimera (see Methods section) to direct the formation of aggregates of DNA functionalized AuNPs. Gold nanoparticles, 10 nm in diameter, were functionalized with two types of noncomplementary ssDNA, A and B (A-AuNPs and B-AuNPs), respectively (sequences shown in the Methods section). Assembly of noncomplementary particles is carried out in a stepwise fashion: a 26 bp duplex is formed between A-DNA strands on a particle and complementary A′-DNA (Figure 1), followed by the invasion of the terminal 10 base pairs of the duplex by the PNA tale of PNA–DNA-1 (Figure 1), where the PNA binds to the A′-DNA strand. Finally, B-AuNPs are hybridized to the 15 base DNA side of PNA–DNA-1 (Figure 1). At each assembly step, the DNA and PNA

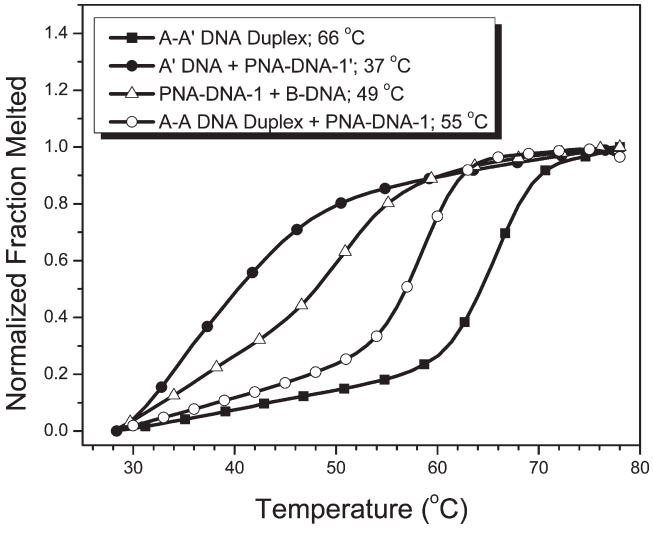

Figure 2. UV melting profiles (heating ramps) of DNA and PNA-DNA components for nanoparticle assembly. The concentration of each strand was 1 μM, and samples were prepared in 0.1 M sodium chloride, 10 mM sodium phosphate buffer, pH 7.0. The T_m values for the different components were determined from the first derivative of the melting curve and are indicated in the figure legend.

modified samples were collected by centrifugation. The specific amounts for each component and specific hybridization times are discussed in the Methods section. In this process, a quaternary complex is formed between the A-DNA sequences on the A-AuNPs, the complementary A′-DNA, the PNA−DNA-1 chimera, and the B-AuNPs.

Prior to examining PNA-invasion of duplex DNA for directed nanoparticle assembly, we studied the thermal stability of the components of the quaternary complex formed by UV−vis spectroscopy. Samples containing equimolar amounts of PNA−DNA-1 and complementary oligonucleotides at 1 μM strand concentration each were prepared in 0.1 M sodium chloride, 10 mM sodium phosphate buffer, and their UV-absorption at 260 nm was monitored for both a cooling and heating ramp. The 26 bp duplex formed by A−A′ DNA duplex, which contains the 10 base PNA recognition site, dissociates at a melting temperature (T_m) of 66 °C, and the binding of PNA−DNA-1 to this duplex results in destabilization characterized by an 11 °C decrease in T_m (Figure 2). However, the shape of the melting curve indicates that invasion by PNA−DNA-1 does not significantly disrupt the duplex structure. Figure 2 also shows the melting profile of PNA−DNA-1 with the single-stranded 26 base DNA oligonucleotide (A′-DNA) containing the 10 base PNA binding site. The recognition site is A-T rich and as a result the melting transition, with an average T_m = 37 °C, is broad compared to that of the invasion complex. The 15 base duplex formed between B-DNA and the 15 base DNA complement of PNA−DNA-1 dissociates at T_m = 49 °C, which should allow for the formation of stable nanoparticle assemblies at room temperature.

The aggregate structures formed by PNA-directed assembly of noncomplementary AuNPs were studied by transmission electron microscopy (TEM) and dynamic light scattering (DLS) without any further purification. Figure 3A shows a typical TEM micrograph, illustrating the formation of nanoparticle clusters. A representative statistical analysis based on TEM observations (Figure 3B) revealed that ~80% of nanoparticles were assembled into larger aggregates (Figure 3D) containing from tens to hundreds of nanoparticles. Control experiments, where PNA−DNA-1 was not added, clearly show no clustering behavior and only isolated particles were observed by TEM (Figure 3C). This conclusion is strongly supported by dynamic light scattering measurements. DLS profiles (Figure 3E), determined in the terms of the volume-averaged hydrodynamic diameter (D_h) population, exhibit successful cluster formation for chimera-mediated assembly, whereas control samples that do not have chimera present remain as separated particles. The sample assembled *via* the PNA invasion approach demonstrates a population with D_h ranging from 100 to about 500 nm, suggesting the existence of the larger-scale aggregates. Moreover, a statistical analysis based on the DLS profile reveals a

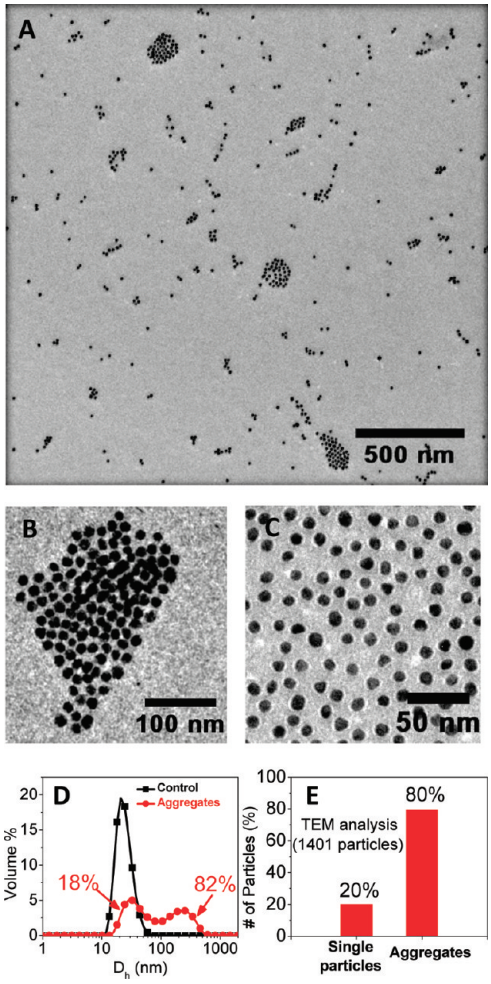

Figure 3. Assembly of noncomplementray gold particles *via* PNA invasion on AuNP surface. (A) Representative low-magnification TEM micrograph. (B) High magnification TEM micrograph of the same sample depicted in panel A of assembled aggregates. (C) TEM micrograph of the control sample, in which no PNA−DNA chimera is added. (D) Statistical analysis of the TEM micrograph. The result suggests that ~80% of particles are assembled into aggregates (n = 1401 particles). (E) DLS measurements of D_h (hydrodynamic diameter) of single particles (control, black) and assembled aggregates (red). The quantitative analysis of the DLS curve reveals that ~82% of the particles have been assembled into aggregates.

yield of 83% of assembled aggregates, agreeing well with our TEM conclusions. The control sample shows a single population at $D_h \approx 25$ nm, similar to the DNA-functionalized AuNPs (see Supporting Information, Figure S1). Similar results were obtained for systems in which PNA−DNA-2, which has a shorter 10 bp DNA recognition sequence, was used for assembly at 4 °C. (see Supporting Information, Figure S2).

The results of TEM and DLS characterization reveal that the PNA−DNA chimeras successfully mediate the assembly of mesoscale aggregates containing up to hundreds of nanoparticles per cluster. The range of aggregate sizes can be attributed to a limited number of chimeras that successfully invade the dsDNA. To examine the binding efficiency of PNA−DNA-1 to A-AuNPs we

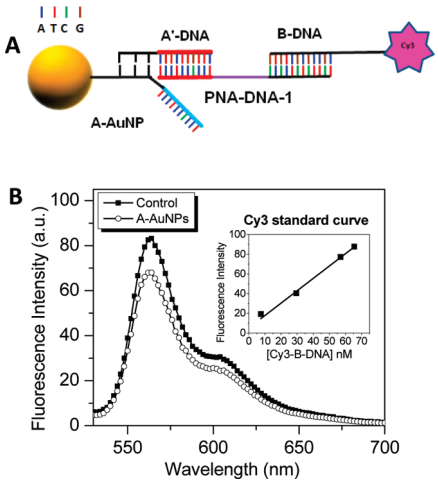

Figure 4. Determination of the invasion efficiency of PNA−DNA-1 on A-AuNP surface. (A) Schematic of method used to determine invasion efficiency. (B) Fluorescence spectra of the supernatant of A-AuNP bound PNA−DNA-1 tagged with Cy3-B-DNA (open circles) and the supernatant of the control sample (without PNA invasion, black). The number of PNA invasion on A-AuNPs is determined by subtracting the fluorescence intensity of A-AuNPs from the control. The inset figure in panel B is the standard fluorescence curve as a function of Cy3-B-DNA concentration.

performed steps similar to the method outlined in Figure 1, except that a DNA with a fluorescent dye, Cy3, (Cy3-DNA-B) was added instead of B-AuNPs. Hybridized Cy3-DNA-B, bound to the Au nanoparticles, was removed by centrifugation, and the decrease in fluorescence of the supernatant was used to determine that approximately 2 to 3 PNA−DNA chimeras bind per nanoparticle (Figure 4), which is consistent with the abundance of smaller clusters compared to macroscopic aggregates observed in TEM images and DLS data. PNA recognition of duplex DNA requires sufficient free energy for invasion, and has been limited to purine and pyrimidine-rich targets. Successful invasion of mixed DNA sequences has been demonstrated, but often requires modifications of the PNA backbone.[30] Here, the PNA−DNA chimeras invade at the terminus of the duplexes packed on the particle surface. The geometrical constrains of the surface compared to free molecules in solution impose barriers for base-pairing. Particularly, we observed the efficiency of A′-DNA hybridization to A-DNA attached to AuNP to be about 26% (∼ 13 DNA per particle). This indicates that a relatively dense packing of ssDNA on particle surface, ∼6 nm^2 per strand, causes an entropic penalty for penetration of complementary strands and their hybridization. The geometrical constraints are further increased when double helixes are formed due to the tighter packing. Therefore, it is remarkable that the PNA invasion process is not significantly affected, and its efficiency is similar to that of complementary A′-DNA strands, ∼20%.

Duplex DNA structures formed between target DNA and DNA-functionalized AuNPs typically exhibit sharp melting profiles and increased melting temperatures in aggregate assemblies compared to those observed for

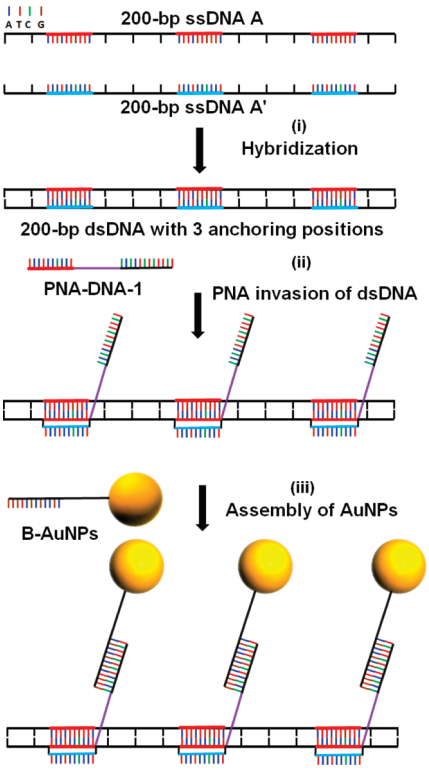

Figure 5. PNA-directed AuNP assembly along a 200 bp dsDNA template. (i) Complementary 200 base DNA sequences are annealed to form a duplex. The DNA duplex has three identical anchoring positions which contain recognition sites for the 10 base PNA of PNA−DNA-1. (ii) Subsequently, PNA−DNA-1 is added, and invasion allows for the binding of up to three chimeras. (iii) B-AuNPs functionalized with the DNA sequence that is complementary to the 15 base DNA region of PNA−DNA-1 are introduced. Nanoparticle trimers can thus be ideally assembled along the dsDNA template.

single complementary DNA strands.[31] The melting process, probed by UV−vis spectroscopy, for a 1 μM solution of a 15 bp DNA duplex formed between PNA−DNA-1 and single-stranded B-DNA shows a broad melting profile, and the duplex melts with a T_m= 49 °C (Figure 2 and Supporting Information, Figure S3A). Temperature dependent DLS was used to determine the melting transition of the PNA-directed aggregate assemblies (Supporting Information, Figure S3B). Here, the concentration of DNA is 200-fold less than in UV−vis melting experiments. The melting transition of the nanoparticle-linked 15 bp DNA duplex occurs at a similar temperature (T_m= 45 °C) and is in agreement with that obtained for the 15 bp DNA duplex formed between the DNA of the chimera and complementary B-DNA, and the melting profile is sharper than that observed for the duplex in the absence of nanoparticles, which is due to the hybridization cooperativity.[32] The comparative UV−vis and DLS melting transitions further support the formation of PNA-directed particle−particle assembly.

To achieve the by-design placement of nano-objects on double-stranded DNA, we used the discussed PNA invasion strategy to assemble AuNPs along a 200 bp DNA template (Figure 5). A 200 bp duplex was designed

with three identical PNA binding sites consisting of 10 base pairs, located at positions 28−37, 96−105, and 164−173 along the duplex (sequence in the Methods section). The 200 bp duplex was formed through hybridization of two complementary 200 bp ssDNA fragments (200 bp ssDNA A and A′). Gel electrophoresis confirmed complete hybridization of the complementary ssDNA into a duplex structure (Supporting Information, Figure S4). In contrast to the previous experiment, the PNA binding sites are not at the termini of the duplex (located at 27 base pairs, ∼10 nm, from both ends), but rather evenly spaced throughout the duplex (58 base pair separation, ∼20 nm spacing in between adjacent binding sites), assuring sufficient space for attaching three 10-nm AuNPs. The chimera's PNA end invades the duplex at the designated positions along the 200 bp sequence, while the chimera's DNA terminus subsequently provides three anchoring positions for B-AuNPs. Thus, ideally, nanoparticle trimers should be assembled along the dsDNA duplex (Figure 5).

Representative TEM micrographs, shown in Figure 6A, reveal that the structures formed contain a mixture of isolated particles, dimers, trimers, and a small fraction of larger clusters. A statistical analysis based on TEM imaging (Figure 6C) provides assembly yields for formed structures: (i) 23% trimers corresponding to ideally assembled structures, (ii) 24% dimers that represent a population of dsDNA which reacted only with two chimeras and/or two particles, (iii) 21% larger clusters (4−10 particles) which are likely formed due to the cross-linking of particles reacting with more than one chimera on different dsDNA, and (iv) 32% single nanoparticles, a fraction of them which might be attached to dsDNA that cannot be visualized on the TEM image. Moreover, more detailed evaluation of trimer clusters reveals all three types of possible configurations of trimers, formed by particles attached to the 200 bp dsDNA laying on a flat surface: (a) straight line, (b) triangle, and (c) "L-shaped" (Figure 6B). DLS measurements obtained from the solutions containing the assembled structures corroborate the formation of nanoparticle clusters by PNA invasion, as shown in Figure 6D. As expected, PNA invasion does not occur when the 200 bp duplex is incubated with PNA−DNA-1 for 12 h at room temperature (Figure S5 in Supporting Information). Invasion of the mixed base 10-mer PNA−DNA chimera requires heating at 50 °C for 12 h and subsequent cooling to room temperature. The melting temperature of the 200 bp duplex is 77 °C (data not shown), and heating to 50 °C allows the duplex to breathe, thereby facilitating invasion. In addition, we conducted "invasion" experiments with a 200% excess of the nonbinding 200 base DNA strand. This ensured that all of the target binding sites were in their duplexed form. DLS and TEM analyses showed agreement with the results shown in Figure 6 (Figures S6 and S7 in Supporting Information).

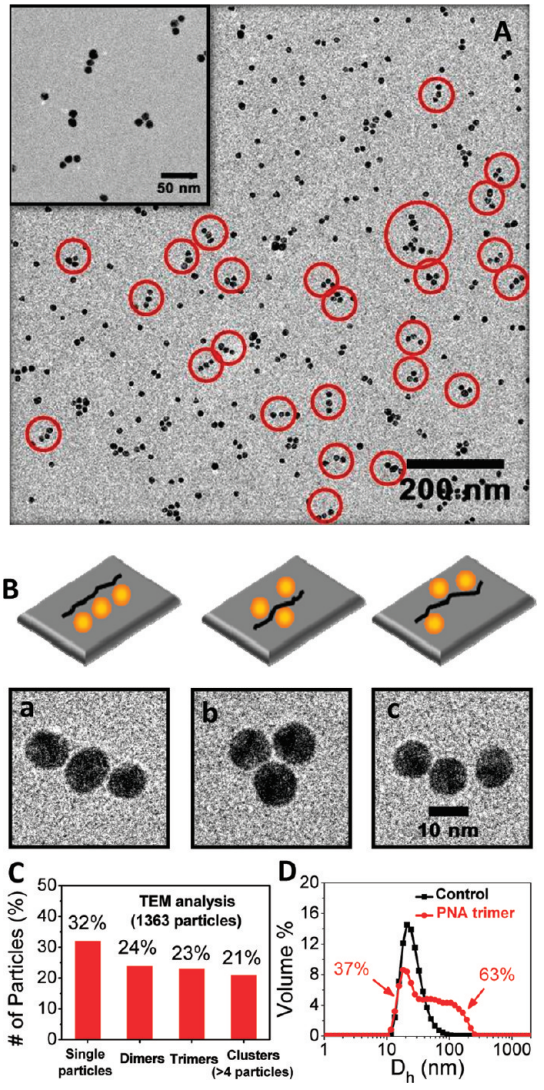

Figure 6. Assembly of nanoclusters based on PNA invasion of 200 bp dsDNA. (A) Representative TEM micrograph of assembled nanoclusters along a 200 bp dsDNA. The red circles indicate the assembled trimers. The insert is a high-magnification TEM image of assembled trimers. (B) Three possible configurations of assembled trimers along the dsDNA template on a flat surface (top, schematic; bottom, TEM images). (C) Statistical analysis based on panel A, suggesting ∼24% dimers, ∼23% trimers, and ∼21% larger clusters assembled (n = 1363 particles). (D) DLS measurements of D_h of single particles (control, black) and assembled clusters (red). The quantitative analysis of the DLS curve reveals that ∼63% of particles have been assembled into clusters.

Analysis of the DLS results demonstrates a yield of 63% nanoparticle clusters, which is consistent with our TEM analysis (68% in total for dimers, trimers, and larger clusters). This indicates the higher efficiency of PNA binding to an isolated duplex compared to the duplexes on a particle, which may be due to the reduced steric constraints. The 23% yield of trimer formation *via* dsDNA template decorated with PNA−DNA chimeras agrees well with theoretically predicted ∼20% yield for scaffold-induced particle clustering in the regime of irreversible binding.[33]

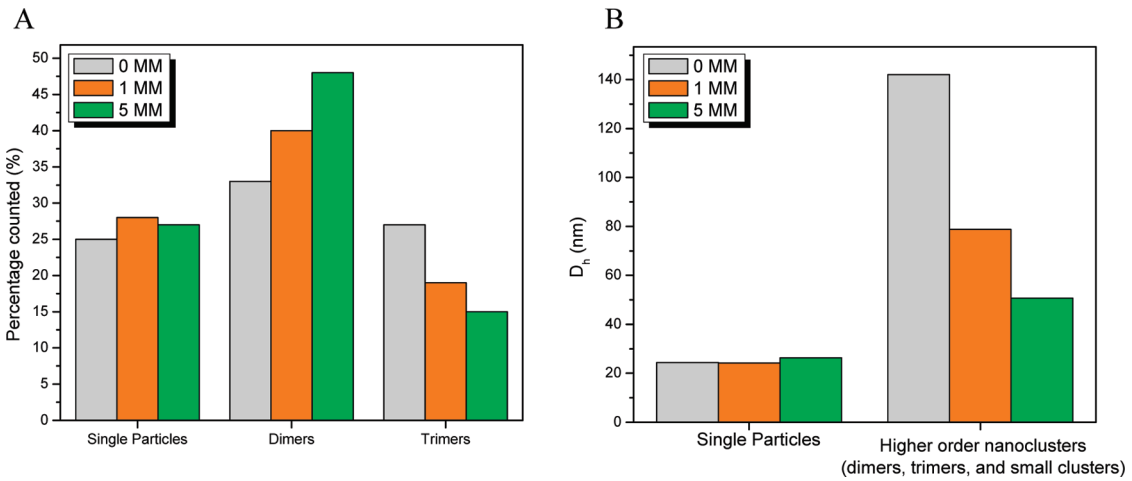

Figure 7. Assembly of nanoclusters based on PNA invasion of 200 bp dsDNA with 0, 1, or 5 mistmatches (MM) in the middle binding site bases 96-105. (A) Analysis of assembled nanoclusters using TEM statistical analysis (representative TEM micrograph Figure S7A). As the number of mismatches increases, the percentage of single particles present remains the same, whereas the percentage of dimers increases and the percentage of trimers decreases. (B) Analysis of assembled clusters using DLS. As the number of mismatches increases, the population of single particles remains the same with an average hydrodynamic radius (D_h) ~25 nm. However, as the number of mismatches increases from 1 to 5, the D_h of the higher order nanocluster population decreases (representative DLS graphs are shown in Figure S7B).

To further confirm that the observed nanoparticle assembly along the 200 bp dsDNA scaffold was caused by PNA invasion of the DNA duplex, a series of control experiments were performed. As expected, samples that do not contain the PNA−DNA chimera fail to form nanoclusters, as was shown by TEM (Supporting Information, Figure S8A). In addition, when the recognition sites are not present, nanoclusters do not form and only single particles are observed by TEM (Supporting Information, Figure S8B). However, samples that contain a mixture of single-stranded 200 base DNA oligonucleotides (with the PNA recognition site), PNA−DNA-1 and the B-AuNPs formed nanoclusters (Supporting Information, Figure S8C). Here no invasion is required and the PNA readily hybridizes to its recognition site. By comparison, TEM indicates similar assembly morphology for the ssDNA and the dsDNA templates.

In order to determine the specificity of PNA invasion for nanocluster assembly along a dsDNA template, we examined the effect of mismatches along the PNA binding site of the duplex in the systems formed with 200% excess of the nonbinding DNA strand. We introduced 0, 1, or 5 mismatches (MM) in the central recognition region spanning bases 96-105 (see Methods section for specific sequences). Using TEM analysis, we observed a decrease in the amount of trimers and higher order nanoclusters and an increase in the amount of dimers by about 15%, as the number of mismatches increased from 1 to 5 (Figure 7A and Figure S7). DLS measurements further supported this conclusion, by demonstration of a nearly 3-fold decrease in the hydrodynamic diameter of the population containing particle clusters (dimers, trimers, and higher order), which signify an enhanced yield of dimer formation. At the same time, the fraction of particle monomers for experiments with mutated 200 bp duplexes remained the same as that observed for unmutated DNA templates (Figure 7B and Figure S7), thus, indicating that mismatches affect redistribution only in the populations of clusters. These experiments with the mutated 200 bp template confirmed that PNA invasion occurs sequence specifically, and the presence of mismatches in the middle binding site created a significant barrier for invasion at this location, thus, resulting in more favorable dimer formation.

In summary, we have demonstrated a new strategy for the assembly of DNA functionalized nanoparticles mediated by the sequence-specific "invasion" of dsDNA duplexes by PNAs. We experimentally demonstrated that this method can be used to direct both particle−particle assembly and by-design placement of nano-objects on dsDNA. We believe that our approach will allow for inclusion of the most regular, stable, readily available and broadly modifiable form of DNA in nanotechnology constructs. Future developments might provide assembly opportunities for the fabrication of diverse nanoarchitectures based on stable DNA duplexes. PNA modifications to improve invasion efficiency and thereof localization of nanoparticles along additional dsDNA templates are currently underway.

METHODS

Materials. DNA oligonucleotides were purchased from Integrated DNA Technologies, Inc. (www.idtdna.com) as lyophilized powders. Unmodified and thoilated oligonucleotides were purified by gel filtration chromatography. Sequences for the DNA strands were

A-DNA: 5′-HS-T_{15}-ACG TCA GAT GTA GAA GGC GTG GAG CTA ATA ACA AT-3

A′-DNA: 5′-ATT GTT ATT AGC TCC ACG CCT TCT AC-3′
B-DNA: 5′-HS-T_{15}-TTC AGA AGA GAT GTG-3′
200 bp ssDNA A: 5′-TCC GCA AGC TGG CCC TCA CTT CAA CGC ATT ATT GTT AAT CTT CCA ATG GGC CAC CTA CCG TAG ACA CGG ACT CTC TAC GCG TTA TGC CTC AGC ATA TTA TTG TTA CTG CGG GAC ATA CGA TAG AGC TTT GCT AAA ATA AGT CCC TGC CTT TCC ACC AAT AGA AAT TAT TGT TAC GTA GCC AAT CGA CGT ATT TGG TAC GT-3′
200 bp ssDNA A′: 5′-ACG TAC CAA ATA CGT CGA TTG GCT ACG TAA CAA TAA TTT CTA TTG GTG GAA AGG CAG GGA CTT ATT TTA GCA AAG CTC TAT CGT ATG TCC CGC AGT AAC AAT AAT ATG CTG AGG CAT AAC GCG TAG AGA GTC CGT GTC TAC GGT AGG TGG CCC ATT GGA AGA TTA ACA ATA ATG CGT TGA AGT GAG GGC CAG CTT GCG GA-3′
Three PNA binding positions for all sequences are underlined.

PNA−DNA chimera's were synthesized and purchased from Bio-Synthesis Inc. as lyophilized powders. The chimeras were purified by HPLC. Sequences for the chimeras were
PNA−DNA-1: 5′-TAA TAA CAA T−linker−T_{15}-CAC ATC TCT TCT GAA-3′
The PNA is underlined and is written from N−C and the DNA is written from 5′-3′. The linker is
cysteine-SMCC-C6 amino
MM 1: ATTATT**A**TTA (corresponding to bases 96-105, mismatch shown in bold)
MM 5: ATT**CGGAC**TA (corresponding to bases 96-105, mismatches shown in bold)

Au Nanoparticle Synthesis. Au nanoparticles of 10-nm were synthesized through a classic citrate reduction method with slight modifications. Briefly, 1 mM $HAuCl_4$ aqueous solution was first heated to boil for 20−30 min. Subsequently, 10 mL of trisodium citrate solution with a concentration of 38 mM was added to the above solution. The reaction was allowed to react until the initial color changed to red, and was then quenched by deionized water. After cooling to room temperature, the Au nanoparticle solution was stored in a glass bottle at ambient conditions for further functionalization with DNA. The particle size was examined by DLS and TEM and the concentration was determined through UV−vis absorption at $\lambda = 519$ nm with an extinction coefficient of 1.0×10^8 L·mole^{-1}·cm^{-1}.

UV−Visible Melting. Concentrations for DNA strands and the PNA−DNA chimera were determined by UV absorbance at 260 nm using a Perkin-Elmer Lamda 35 UV−vis spectrometer. For UV melting experiments, 1 μM of each strand was mixed and UV−vis absorbance at 260 nm was recorded at the rate of 1 °C/min for both the heating and cooling runs. Melting temperatures (T_m) were determined by taking the first derivative of the absorbance *versus* temperature profile.

Functionalization of Au Nanoparticles. Before DNA loading, the thiol functionality was deprotected by the addition of 0.1 M dithiothretol (DTT) for at least 2 h on ice (typically, 10−11 OD of concentrated DNA; 200 μL of DTT). The deprotected DNA solutions were purified using desalting NAP-5 columns (Sephadex G-25, Amersham Biosciences). Au nanoparticles were functionalized with deprotected thiol-oligonucleotides following methods for high DNA coverage reported by Mirkin and co-workers. In a typical experiment with 10 nm gold nanoparticles, an aliquot (1−50 μL) of a purified DNA 50−300 μM solution was added to a 1 mL aliquot of gold particles (10−30 nM). The ssDNA and particle solutions were incubated at room temperature in a nonbuffered solution for at least 3 h before adding phosphate buffer to bring its concentration to 10 mM (pH = 7.4). The solution was left to anneal at 25 °C for 4 h before the addition of NaCl (0.025 M). The salt concentration was then increased gradually from 0.025 to 0.3 M NaCl over 24 h, and left to anneal for an additional 24 h at 0.3 M. The excess DNA next was removed from the solutions by centrifugation for 30 min at 4500*g* (3×).

PNA-Directed Assembly of Aggregates. The molar concentration of AuNP probes was measured by UV−vis spectroscopy (molar extinction coefficient 1.0×10^8 M^{-1} cm^{-1} at 524 nm). A 15 nM (50 uL) solution of AuNPs functionalized with A-DNA strands was mixed with a 60-fold excess of A′ cDNA (900 nM). The solution was heated to 65 °C for 10 min and cooled to room temperature. Unhybridized A′-DNA was removed by centrifugation. A 60-fold excess of PNA−DNA chimera (900 nM) was added, and the solution was heated to 50 °C for 10 min and cooled to room temperature. Unbound PNA was removed by centrifugation. Here the PNA recognition site is on the A′-DNA strand. The PNA−DNA chimera will only bind to hybridized A′-DNA. An equal molar ratio of B-AuNPs (15 nM)/A-AuNPs was added. The solution was allowed to sit overnight at room temperature. The samples were analyzed without further purification.

PNA-Directed Assembly of Nanoparticle Trimers. Equal molar concentration of 200 bp DNA A and its complementary strand, 200 bp DNA A′, were first mixed in 0.1 M PBS and annealed for hybridization at 80 °C for overnight. Subsequently a 3-fold excess of PNA−DNA chimera was added and the solution was allowed to anneal at 50 °C for overnight. A 3-fold excess of B-AuNPs to the dsDNA in 0.1 M PBS was then added to the above solution and heated to 65 °C for 10 min and then cooled to room temperature for overnight. The nanoclusters were characterized without further purification.

Three control experiments were performed under the same condition to the above experiment except that (1) no PNA−DNA chimera was added, (2) no 200 bp DNA A was added, and (3) no 200 bp DNA A′ was added, respectively.

Characterization of Aggregates and Trimers. *Dynamic Light Scattering (DLS).* DLS measurements were performed on a Malvern Zetasizer ZS instrument. The instrument is equipped with a 633 nm laser source and a backscattering detector at 173°.

Transmission Electron Microscopy (TEM). TEM micrographs of DNA-functionalized Au NPs and assembled aggregates and nanoclusters were collected using a JEOL 1300 transmission electron microscope operated at 120 kV. Samples were prepared by placing a droplet of the aqueous solution onto a 400-mesh carbon-coated copper grid, followed by drying at room temperature for overnight before imaging.

Temperature-Dependent DLS. DLS measurements were recorded for aggregate samples at a rate of 1 °C/min, with measurements taken every 4 °C. Prior to measurement recording samples were equilibrated for 5 min. Melting temperatures (T_m) were determined by taking the first derivative of the absorbance *vs* temperature profile.

Quantitation of Hybridized PNA−DNA Chimeras. To determine the number of hybridized PNA−DNA chimeras, which were partially complementary to nanoparticle-hybridized A′-DNA oligonucleotides, a 15 nM (50 uL) solution of AuNPs functionalized with A-DNA strands was mixed with a 60-fold excess of A′ cDNA (900 nM). The solution was heated to 65 °C for 10 min and cooled to room temperature. Unhybridized A′-DNA was removed by centrifugation. A 60-fold excess of PNA−DNA chimera (900 nM) was added, and the solution was heated to 50 °C for 10 min and cooled to room temperature. Unbound PNA was removed by centrifugation. Here the PNA recognition site is on the A′-DNA strand. The PNA−DNA chimera will only bind to hybridized A′-DNA. A 60-fold excess of Cy3-B-DNA was added and allowed to hybridize at room temperature overnight. The samples were centrifuged to remove unbound Cy3-B-DNA, and the fluorescence of the supernatant was analyzed using a Varian fluorimeter.

Acknowledgment. Research was supported by the U.S. Department of Energy, Basic Energy Sciences, Materials Sciences and Engineering Division. Research was carried at the Center for Functional Nanomaterials, Brookhaven National Laboratory, which is supported by the U.S. Department of Energy, Office of Basic Energy Sciences, under Contract No. DE-AC02-98CH10886. We thank C. Chi for nanoparticle synthesis.

Supporting Information Available: Additional TEM and DLS data for single particle, aggregate-directed assembly and nanoclusters formed on 200 bp templates, thermal melting curves for AuNP aggregates measured by DLS, and gel electrophoresis of 200 bp duplex. This material is available free of charge *via* the Internet at http://pubs.acs.org.

REFERENCES AND NOTES

1. Mirkin, C. A.; Letsinger, R. L.; Mucic, R. C.; Storhoff, J. J. A DNA-Based Method for Rationally Assembling Nanoparticles into Macroscopic Materials. *Nature* **1996,** *382,* 607–609.
2. Alivisatos, A. P.; Johnsson, K. P.; Peng, X. G.; Wilson, T. E.; Loweth, C. J.; Bruchez, M. P.; Schultz, P. G. Organization of

'Nanocrystal Molecules' Using DNA. *Nature* **1996,** *382*, 609–611.
3. Le, J. D.; Pinto, Y.; Seeman, N. C.; Musier-Forsyth, K.; Taton, T. A.; Kiehl, R. A. DNA-Templated Self-Assembly of Metallic Nanocomponent Arrays on a Surface. *Nano Lett.* **2004,** *4*, 2343–2347.
4. Zheng, J. W.; Constantinou, P. E.; Micheel, C.; Alivisatos, A. P.; Kiehl, R. A.; Seeman, N. C. Two-Dimensional Nanoparticle Arrays Show the Organizational Power of Robust DNA Motifs. *Nano Lett.* **2006,** *6*, 1502–1504.
5. Nykypanchuk, D.; Maye, M. M.; van der Lelie, D.; Gang, O. DNA-Guided Crystallization of Colloidal Nanoparticles. *Nature* **2008,** *451*, 549–552.
6. Xiong, H. M.; van der Lelie, D.; Gang, O. DNA Linker-Mediated Crystallization of Nanocolloids. *J. Am. Chem. Soc.* **2008,** *130*, 2442–2443.
7. Hill, H. D.; Macfarlane, R. J.; Senesi, A. J.; Lee, B.; Park, S. Y.; Mirkin, C. A. Controlling the Lattice Parameters of Gold Nanoparticle FCC Crystals with Duplex DNA Linkers. *Nano Lett.* **2008,** *8*, 2341–2344.
8. Park, S. Y.; Lytton-Jean, A. K. R.; Lee, B.; Weigand, S.; Schatz, G. C.; Mirkin, C. A. DNA-Programmable Nanoparticle Crystallization. *Nature* **2008,** *451*, 553–556.
9. Maye, M. M.; Nykypanchuk, D.; Cuisinier, M.; van der Lelie, D.; Gang, O. Stepwise Surface Encoding for High-Throughput Assembly of Nanoclusters. *Nat. Mater.* **2009,** *8*, 388–391.
10. Sharma, J.; Ke, Y. G.; Lin, C. X.; Chhabra, R.; Wang, Q. B.; Nangreave, J.; Liu, Y.; Yan, H. DNA-Tile-Directed Self-Assembly of Quantum Dots into Two-Dimensional Nanopatterns. *Angew. Chem., Int. Ed.* **2008,** *47*, 5157–5159.
11. Chen, Y.; Liu, H. P.; Ye, T.; Kim, J.; Mao, C. D. DNA-Directed Assembly of Single-Wall Carbon Nanotubes. *J. Am. Chem. Soc.* **2007,** *129*, 8696–8697.
12. Mastroianni, A. J.; Claridge, S. A.; Alivisatos, A. P. Pyramidal and Chiral Groupings of Gold Nanocrystals Assembled Using DNA Scaffolds. *J. Am. Chem. Soc.* **2009,** *131*, 8455–8459.
13. Hung, A. M.; Micheel, C. M.; Bozano, L. D.; Osterbur, L. W.; Wallraff, G. M.; Cha, J. N. Large-Area Spatially Ordered Arrays of Gold Nanoparticles Directed by Lithographically Confined DNA Origami. *Nat. Nanotechnol.* **2010,** *5*, 121–126.
14. Sharma, J.; Chhabra, R.; Cheng, A.; Brownell, J.; Liu, Y.; Yan, H. Control of Self-Assembly of DNA Tubules through Integration of Gold Nanoparticles. *Science* **2009,** *323*, 112–116.
15. Biancaniello, P. L.; Crocker, J. C.; Hammer, D. A.; Milam, V. T. DNA-Mediated Phase Behavior of Microsphere Suspensions. *Langmuir* **2007,** *23*, 2688–2693.
16. Maye, M. M.; Nykypanchuk, D.; van der Lelie, D.; Gang, O. DNA-Regulated Micro- and Nanoparticle Assembly. *Small* **2007,** *3*, 1678–1682.
17. Leunissen, M. E.; Dreyfus, R.; Sha, R.; Seeman, N. C.; Chaikin, P. M. Quantitative Study of the Association Thermodynamics and Kinetics of DNA-Coated Particles for Different Functionalization Schemes. *J. Am. Chem. Soc.* **2010,** *132*, 1903–1913.
18. Cohen, J. D.; Sadowski, J. P.; Dervan, P. B. Programming Multiple Protein Patterns on a Single DNA Nanostructure. *J. Am. Chem. Soc.* **2008,** *130*, 402–403.
19. Demidov, V. V.; Yavnilovich, M. V.; Belotserkovskii, B. P.; Frankkamenetskii, M. D.; Nielsen, P. E. Kinetics and Mechanism of Polyamide (Peptide) Nucleic-Acid Binding to Duplex DNA. *Proc. Natl. Acad. Sci. U.S.A.* **1995,** *92*, 2637–2641.
20. Lohse, J.; Dahl, O.; Nielsen, P. E. Double Duplex Invasion by Peptide Nucleic Acid: A General Principle for Sequence-Specific Targeting of Double-Stranded DNA. *Proc. Natl. Acad. Sci. U.S.A.* **1999,** *96*, 11804–11808.
21. Peffer, N. J.; Hanvey, J. C.; Bisi, J. E.; Thomson, S. A.; Hassman, C. F.; Noble, S. A.; Babiss, L. E. Strand-Invasion of Duplex DNA by Peptide Nucleic-Acid Oligomers. *Proc. Natl. Acad. Sci. U.S.A.* **1993,** *90*, 10648–10652.
22. Chakrabarti, R.; Klibanov, A. M. Nanocrystals Modified with Peptide Nucleic Acids (PNAs) for Selective Self-Assembly and DNA Detection. *J. Am. Chem. Soc.* **2003,** *125*, 12531–12540.
23. Gourishankar, A.; Shukla, S.; Ganesh, K. N.; Sastry, M. Isothermal Titration Calorimetry Studies on the Binding of DNA Bases and PNA Base Monomers to Gold Nanoparticles. *J. Am. Chem. Soc.* **2004,** *126*, 13186–13187.
24. Murphy, D.; Redmond, G.; de la Torre, B. G.; Eritja, R. Hybridization and Melting Behavior of Peptide Nucleic Acid (PNA) Oligonucleotide Chimeras Conjugated to Gold Nanoparticles. *Helv. Chim. Acta* **2004,** *87*, 2727–2734.
25. Lytton-Jean, A. K. R.; Gibbs-Davis, J. M.; Long, H.; Schatz, G. C.; Mirkin, C. A.; Nguyen, S. T. Highly Cooperative Behavior of Peptide Nucleic Acid-Linked DNA-Modified Gold-Nanoparticle and Comb-Polymer Aggregates. *Adv. Mater.* **2009,** *21*, 706–709.
26. Kanjanawarut, R.; Su, X. D. Colorimetric Detection of DNA Using Unmodified Metallic Nanoparticles and Peptide Nucleic Acid Probes. *Anal. Chem.* **2009,** *81*, 6122–6129.
27. Su, X. D.; Kanjanawarut, R. Control of Metal Nanoparticles Aggregation and Dispersion by PNA and PNA−DNA Complexes, and Its Application for Colorimetric DNA Detection. *ACS Nano* **2009,** *3*, 2751–2759.
28. Nielsen, P. E. Sequence-Selective Targeting of Duplex DNA by Peptide Nucleic Acids. *Curr. Opin. Mol. Ther.* **2010,** *12*, 184–191.
29. Pellestor, F.; Paulasova, P.; Hamamah, S. Peptide nucleic acids (PNAs) as diagnostic devices for genetic and cytogenetic analysis. *Curr. Pharm. Des.* **2008,** *14*, 2439–2444.
30. Rapireddy, S.; He, G.; Roy, S.; Armitage, B. A.; Ly, D. H. Strand Invasion of Mixed-Sequence B-DNA by Acridine-Linked, Gamma-Peptide Nucleic Acid (γ-PNA). *J. Am. Chem. Soc.* **2007,** *129*, 15596–15600.
31. Zhang, X.; Ishihara, T.; Corey, D. R. Strand Invasion by Mixed Base PNAs and a PNA−Peptide Chimera. *Nucleic Acids Res.* **2000,** *28*, 3332–3338.
32. Jin, R. C.; Wu, G. S.; Li, Z.; Mirkin, C. A.; Schatz, G. C. What Controls the Melting Properties of DNA-Linked Gold Nanoparticle Assemblies? *J. Am. Chem. Soc.* **2003,** *125*, 1643–1654.
33. Licata, N. A.; Tkachenko, A. V. How to Build Nanoblocks Using DNA Scaffolds. *Europhys. Lett.* **2008,** *84*, 20010–20014.